Adaptive Harmonic Power Flow Algorithm for Hybrid AC/DC Transmission Systems

Yifu Li, *Graduate Student Member, IEEE,* Shiyuan Wang, Amir H. Etemadi, *Member, IEEE,* and Payman Dehghanian, *Senior Member, IEEE*

***Abstract*—With the continuous integration of new generation resources and evolving load profiles in modern power systems, the harmonic pollution in the electric power network is continuously on the rise. This level of waveform distortion in the electric power system and its impact on the operation of different components can no longer be neglected in high-voltage power systems. In this paper and beyond the state-of-the-art, an adaptive frequency-domain-based harmonic power flow (HPF) analytic is proposed for power systems with voltage source converter (VSC)-based high-voltage direct current (HVDC) transmission lines. The hybrid nonlinear model can be applied to both fundamental and harmonic power flow analyses at the point of common coupling. To demonstrate the effectiveness of the proposed HPF algorithm in hybrid AC/DC transmission systems, a modified pulse width modulation (PWM)-controlled bi-terminal VSC-HVDC transmission system based on the IEEE 30-bus test system is used as a testbed. Simulation results and numerical analysis verify the effective performance of the proposed solution as compared to the traditional approaches.**

***Index Terms*—harmonic power flow (HPF); high-voltage direct-current (HVDC); pulse width modulation (PWM); voltage source converter (VSC).**

I. Introduction

WITH the growing integration of new energy sources and larger loads with more complex profiles, harmonic analysis and power quality evaluation have become more and more important in modern power systems [1]. As one main component of the high-voltage direct-current (HVDC) systems and flexible AC transmission system (FACTS), voltage source converters (VSCs) have been widely used as the AC/DC hybrid grid developments evolve. Focused on the HVDC part, the main advantages of using VSC compared to other conventional control technologies, such as line-commutated converter (LCC), include the ability to independently control the active and reactive power, black-start capability, and faster damping support [2]. However, due to their switching characteristics, VSCs are one main harmonic sources in HVDC systems, that if not properly managed, could challenge the power system operation with the growing likelihood of protective relay maloperations and equipment aging acceleration [3].

Harmonic analysis is essential to control and mitigate the potential risk to power system protection. As early as 1989, K. Olejniczak, et al. have discussed the basic mechanisms of generation and flow of harmonic signals in unbalanced power systems with a six-pulse converter as the non-linear load [4]. The evolution of variable frequency drives (VFDs) have played a key role in promoting HVDC technological innovation. HVDC transmission using VSCs with pulse-width modulation (PWM) was introduced in the late 1990's, which replaced the conventional thyristor valves with more modern components such as insulated-gate bipolar transistor (IGBT) valves [5]. In 2004, Li Gengyin, et al. proposed a novel algorithm for power flow (PF) calculation based on equivalent injection power in VSC-HVDC systems [6]. In 2013, Mohamadreza Baradar, et al. proposed a multi-option power flow approach for hybrid AC/DC power grids [7]. In 2016, Runze Chai, et al. proposed a unified power flow algorithm based on the Newton-Raphson method to find a feasible solution in hybrid AC/DC grids incorporating VSCs [8]. Because VSCs generate harmonics under unbalanced conditions [9], in 2016, Bo Liu, et al. extended the traditional HPF models to include VSC-based HVDC lines [10]. In 2017, Haytham M. A. Ahmed, et al. proposed a unified load flow model for AC/DC hybrid power distribution systems [11]. In 2019, Ruirui, et al. presented a comprehensive analytical analysis of the AC- and DC-side harmonics of the three-level active neutral point clamped inverter with a space vector modulation (SVM) scheme [12]. The work was motivated due to the fact that space vector PWM (SVPWM) provides a more efficient use of supply voltage, generates less total harmonic distortion (THD), and reduces harmonic content in the output voltage waveforms than the sinusoidal PWM (SPWM) method [13].

Switching function is often the first issue and the most tricky problem when analyzing power systems that include converters with complex structures, especially when analyzing power flow as different switching strategies for power electronic converters would lead to different outcomes. So far, the three main methods in addressing this challenge are through Fourier coefficients, harmonic elimination, and PWM [1], [14], [15].

In this paper, a new hybrid AC/DC power system, based on the IEEE 30-bus transmission system (hereafter referred to as 30-HVDC system), is established with a PWM-controlled bi-terminal VSC-HVDC station included. VSCs in HVDC are regarded as the only harmonic source in power system. An adaptive HPF algorithm is proposed to analyze the power flow across the system under harmonic conditions. The rest of the paper is structured as follows: Section II introduces a background on the VSC-HVDC transmission station used for harmonic analysis, a switching function method, the control strategies of the VSC-HVDC transmission station, and some basic assumptions used in our research. Section III implements

This work was supported in part by the National Science Foundation (NSF) under Grant ECCS-1610390.

Y. Li, and P. Dehghanian are with the Department of Electrical and Computer Engineering, George Washington University, Washington, DC 20052, USA (e-mails: liyifu@gwu.edu; payman@gwu.edu).

A. H. Etemadi is with the Department of Engineering Management and Systems Engineering, George Washington University, Washington, DC 20052, USA (e-mail: etemadi@gwu.edu).

S. Wang is with Quanta Technology, LLC., Raleigh, NC 27607, USA (e-mail: shiyuan1225@gmail.com).

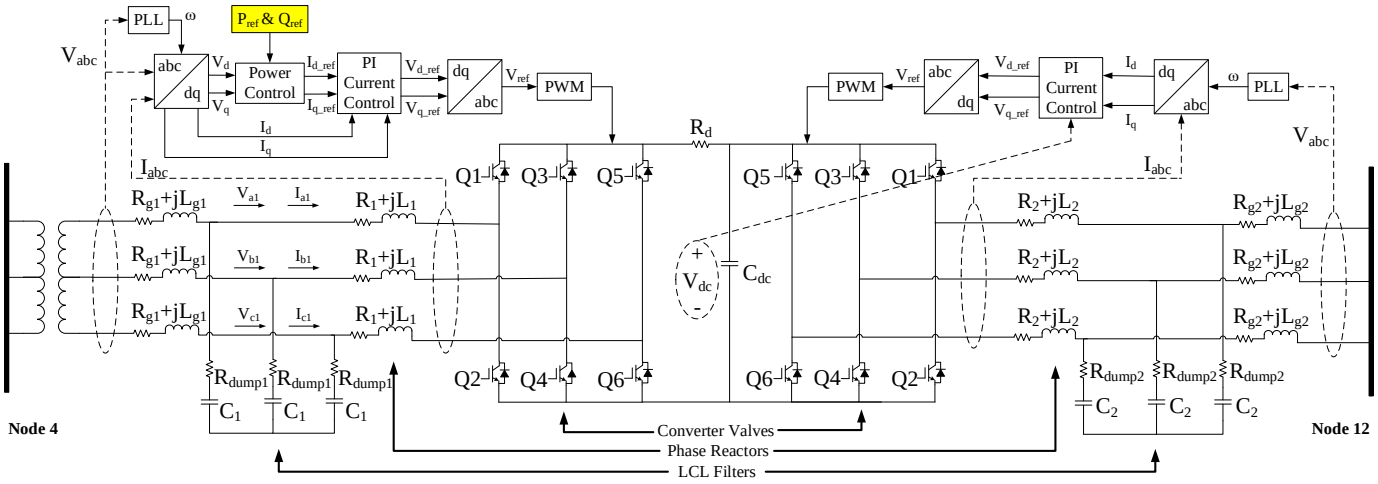

Fig. 1. Two-level NSPWM controlled bi-terminal VSC-HVDC transmission system.

the mathematical models of the developed 30-HVDC system and the proposed adaptive HPF algorithm framework. Section IV presents the numerical studies of the fundamental PF and the proposed HPF algorithms in the 30-HVDC system. Finally, the conclusions are summarized in Section V.

II. Technical Background

A. NSPWM Controlled Bi-Terminal VSC-HVDC

Here, the naturally-sampled PWM (NSPWM) is used in the VSC-HVDC transmission system, as shown in Figure 1. Both the rectifier and inverter are 3-phase 6-pulse IGBT converter, wherein the P_{ref} and Q_{ref} can be changed manually as the function to adjust the firing angle. The control structure is based on the basic VSC-HVDC model [5], referring to the back-to-back converter case in Typhoon HIL software [16] and the PWM control decision [17], [18]. Phase lock loop (PLL) is used to synchronize frequency and phase with the main grid. LCL filters are specially designed to reduce harmonics of the current absorbed by the power converters [19].

For a 3-phase VSC with the typical 2-level topology [20], the number of times the triangular wave repeats within one sinusoidal fundamental frequency f_1, is called the switching- or carrier frequency $f_{sw} = \omega_{sw}/2\pi$. And $\omega_{sw} = m_f\omega_1$, where frequency modulation ratio m_f is usually a multiple of 3. The ratio of the reference to the triangular carrier wave in VSC is called the modulation index $m_a = V_{reference}/V_{carrier}$. By adjusting the phase angle and m_a of the reference signal, the active and reactive power can be transferred independently through the converter from the AC to DC side, or vice versa [10], [21], [22]. V_{dc} is the boost voltage of the DC circuit, and the AC-side voltage is related to the DC-side voltage as

$$V_{i,LL_{rms}}^{AC} = m_a K_{vsc} V_j^{DC} \tag{1}$$

where the value of converter constant K_{vsc} is dependent on the type of the VSC as well as the type of the PWM strategy [11]. For the 3-phase SPWM converter, $K_{vsc} = \sqrt{3}/2\sqrt{2}$, while for the 3-phase SVPWM converter, $K_{vsc} = \sqrt{2}/2$ [23]–[25].

B. Switching Function

In Figure 1, Q1 to Q6 stand for six converter valves of one 6-pulse IGBT converter. In 2-level PWM, the reference signal (V_{ref} input), also called modulating signal, is compared with a symmetrical triangular wave carrier. In MATLAB Simulink, the 2-level PWM block under natural sampling generates a unipolar switching function. That is, when the reference signal is greater than the carrier, the pulse for the upper switching device is high (1), and the pulse for the lower device is low (0) [26]. We identify the switching function of phase p as [27]:

$$S_p = \begin{cases} 1, \ when\ Q1\ close \\ 0, \ when\ Q1\ open \end{cases}$$

When the carrier signal is a triangular wave, the theoretical switching function prosess of Q1 is shown in Figure 2.

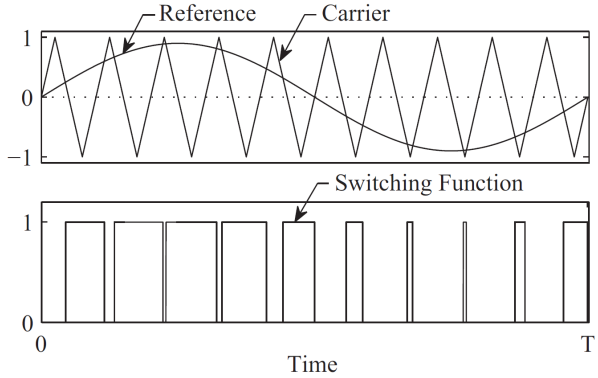

Fig. 2. Theoretical 2-level PWM switching function process of Q1 [10].

In practice, the input reference signal may not be a perfect sinusoidal wave due to LCL filters parameters and resonance features, but the error can be disregarded at a high switching frequency. Assume the reference voltage signal V_{ref} is approximately a sinusoidal wave $f_r(t_k) = m_a \sin(\omega_1 t_k + \Delta\delta_1)$, where amplitude modulation index m_a could be computed from Equation (1) and fundamental angular frequency $\omega_1 = 2\pi f_1$. $\Delta\delta_1$ is the firing angle from Equation (2). t_k (k=1,2,$\cdots$,$2m_f$) denotes the switching instants during one fundamental cycle $T_1 = 1/f_1$.

Note that the modulation ratio m_a would significantly change the switching function. Usually, when $0 < m_a < 1$, the amplitude of the fundamental frequency component varies linearly with m_a. However, when $m_a > 1$, it is called over-modulation. Over-modulation would causes more harmonics in the side-bands [28]. The amplitude of the fundamental frequency component in this case would not vary linearly with the modulation factor; that is the traditional switching function expressed by Bessel function would be no longer accurate.

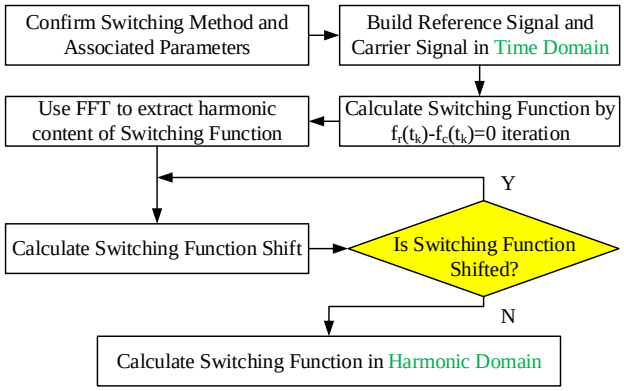

Fig. 3. Switching function calculation in harmonic domain [29].

Following the procedure in Figure 3, where carrier voltage signal is the triangular wave $f_c(t_k)$ as shown in Figure 2, and the switching instants t_k could be solved from $f_r(t_k) - f_c(t_k) = 0$ by the iteration method, the switching function for a single phase p could be simplified as

$$S_p(t) = \begin{cases} 1, & t \in (t_k, t_{k+1}] \\ 0, & \text{else} \end{cases}$$

C. Two VSC Control Strategies

The VSC control strategies vary based on specific system structures. For a classic bi-terminal VSC-HVDC transmission system as the one shown in Figure 1 and Figure 4, there exist two basic control strategies, summarized in Table I [6], [30]. Partial symbols are explained in Section III-A. In this paper, the second control strategy is applied.

TABLE I
TWO CONTROL STRATEGIES FOR A BI-TERMINAL VSC-HVDC SYSTEM

Method	1	2
Fixed Value	V_{S1},V_{S_2}	V_{S1},V_{S_2}
Controlled Value	**VSC1** $M_1 \rightarrow V_{C1}$ **VSC2** $M_2 \rightarrow V_{C2}$ **DC** V_{dc},I_{dc}	**VSC1** P_{C1},Q_{C1} **VSC2** Q_{C2} **DC** V_{dc}
Derived Value	P_{C1},Q_{C1},P_{C2},Q_{C2}	V_{C1},V_{C2},P_{C2}
Target Value	P_{S1},Q_{S1},P_{S2},Q_{S2}	P_{S1},Q_{S1},P_{S2},Q_{S2}

D. Basic Assumptions

Before the derivation of the harmonic model, there are some basic assumptions that have been followed in this paper described in the following [6], [10]:

(i) The hybrid power system has only one slack bus (Bus 1) in the AC system.
(ii) Three-phase AC voltage of the converter bus is a symmetrical sinusoidal waveform.
(iii) The converters operate in balance and symmetrical mode.
(iv) All valves are ideal, and the internal losses of the converters are neglected.
(v) The upper switches (Q1, Q3, Q5) in the other two phase-legs go through the same processes except the reference signals are delayed by 120° and 240°, respectively.
(vi) The only harmonic sources are the VSCs, harmonic current injections of the non-converter AC buses, and the imaginary parts of the DC quantities are all zeros.

III. PROPOSED METHODOLOGY

A. Steady-State Model of the VSC-HVDC

The steady-state model of the VSC-HVDC station with Y-Y winding transformer converters is shown in Figure 4 [6], which could be regarded as a transmission station. The rectifier operates as a "master DC voltage regulator" and the inverter operates as a "power dispatcher" [28]. This model operates under the same principle as the HVDC back-to-back configuration, while the only difference is that the VSCs are connected via transmission DC lines with cable impedance R_d [31]. The $R_{eq1} + jX_{eq1}$ can be calculated as the equivalent load including resistances and filters in the left part in Figure 1, and so does the $Z_{eq2} = R_{eq2} + jX_{eq2}$. Besides, Z_{eq1} and Z_{eq2} would be the main non-linear loads at the converter AC bus when calculating harmonics.

$$Z_{eq1} = R_{eq1} + jX_{eq1}$$
$$= R_{g1} + j2\pi f_1 L_{g1} + \frac{(R_1 + j2\pi f_1 L_1)(R_{dump1} + j\frac{1}{2\pi f_1 C_1})}{R_1 + j2\pi f_1 L_1 + R_{dump1} + j\frac{1}{2\pi f_1 C_1}}$$

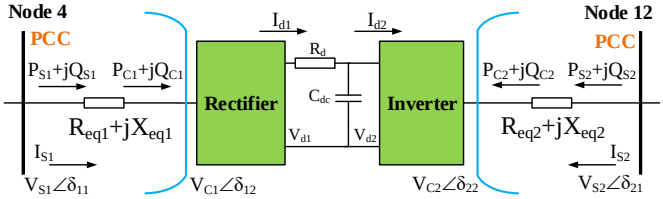

Fig. 4. Steady-state model of the VSC-HVDC transmission station [6].

P_{S1}+jQ_{S1} is the power delivered from node 4, which can be calculated from power flow analysis. The injection power P_{ref}+jQ_{ref} in Figure 1 is presented as P_{C1}+jQ_{C1} in Figure 4 and is to compensate for the phase shifting and to adjust the firing angle. A proper selection of LC parameters, phase reactors, and LCL filters would ideally lead to $\delta_{12} = \delta_{22} = 0°$ [6], which is serving as a power factor compensator (PFC) [32]. Even the adjusted angle is not 0°, it would not affect the overall calculation procedure and the firing angle of the rectifier could be expressed as [6]

$$\Delta\delta_1 = \delta_{11} - \delta_{12} = -tan^{-1}\frac{P_{C1}X_{eq1} - Q_{C1}R_{eq1}}{V_{S1}^2 + P_{C1}R_{eq1} + Q_{C1}X_{eq1}} \quad (2)$$

$P_{S2} + jQ_{S2}$ is the power delivered from node 12. $V_{S1}\angle\delta_{11}$ is the voltage at node 4 through a transformer, and $V_{S2}\angle\delta_{21}$ is the voltage at node 12. R_d is the π-model DC transmission line resistance totaling about $1\,\Omega$. The boost voltage of the

DC circuit V_{d1} can be roughly estimated by Equation (1), i.e. $V_{C1}^{base} = (\sqrt{3}/2\sqrt{2})V_{d1}^{base}$, where V_{d1} is tested as 40 kV in this system, capturing different parameters of the PI controller in the control scheme in Figure 1. Although this value is lower than the typical DC voltage of an HVDC system, it is the maximum magnitude to ensure the convergence under this specific hybrid condition, and it would not affect power flow analysis. Assuming the initial point of common coupling (PCC) voltage at node 4 is higher than that at node 12, the DC current I_{d1} and I_{d2} in the transmission line should follow one direction at the beginning. The steady-state condition of the HVDC-VSC transmission station is achieved when $I_{d1} - I_{d2} = 0$, which results in no DC current flowing into the capacitor C_{dc}.

By adjusting the phase angle difference between the output voltage of the VSC and the PCC voltage, the firing angle $\Delta\delta_1$ can control the active power exchange between AC and DC systems [33]. The reactive power exchanged between the AC system and the VSC is controlled by adjusting the voltage magnitude difference across the coupling transformer, i.e., $|V_{S1}| - |V_{C1}|$, where the active and reactive power injected by the AC system on the rectifier side (with no harmonics) are given by [31]

$$\begin{aligned} P_{C1} \approx & \frac{|V_{S1}|\,|V_{C1}|}{X_{eq1}} \sin\Delta\delta_1 \\ Q_{C1} \approx & \frac{|V_{S1}|^2}{X_{eq1}} - \frac{|V_{S1}|\,|V_{C1}|}{X_{eq1}} \cos\Delta\delta_1 \end{aligned} \tag{3}$$

wherein X_{eq1} is the equivalent reactance of the coupling transformer. Above formula could be used to roughly estimate the adjustment boundary of the firing angle. From Table I, the value of Z_{eq1}, Z_{eq2}, $V_{S1}\angle\delta_{11}$, $V_{S2}\angle\delta_{21}$, R_d, and V_{d1} are given. P_{C1} and Q_{C1} can be manually adjusted by the firing angle $\Delta\delta_1$, and $Q_{C2} = Q_{C1}$. The rectifier-side and inverter-side voltage V_{C1} and V_{C2} can be calculated as [6]

$$V_{C1}^2 = \frac{-(2P_{C1}R_{eq1} + 2Q_{C1}X_{eq1} - V_{S1}^2) + \sqrt{B_1}}{2}$$
$$V_{C2}^2 = \frac{-(2P_{C2}R_{eq2} + 2Q_{C2}X_{eq2} - V_{S2}^2) + \sqrt{B_2}}{2}$$

wherein

$$\begin{aligned} B_1 = & \big(2P_{C1}R_{eq1} + 2Q_{C1}X_{eq1} - V_{S1}^2\big)^2 - 4[(P_{C1}X_{eq1} \\ & -Q_{C1}R_{eq1})^2 + (P_{C1}R_{eq1} + Q_{C1}X_{eq1})^2] \\ B_2 = & \big(2P_{C2}R_{eq2} + 2Q_{C2}X_{eq2} - V_{S2}^2\big)^2 - 4[(P_{C2}X_{eq2} \\ & -Q_{C2}R_{eq2})^2 + (P_{C2}R_{eq2} + Q_{C2}X_{eq2})^2] \end{aligned}$$

Hence, the power at node 4 is

$$P_{S1} = P_{C1} + \frac{(P_{C1}^2 + Q_{C1}^2)R_{eq1}}{V_{C1}^2} \tag{4}$$

$$Q_{S1} = Q_{C1} + \frac{(P_{C1}^2 + Q_{C1}^2)X_{eq1}}{V_{C1}^2} \tag{5}$$

and the power at node 12 is

$$P_{S2} = P_{C2} + \frac{(P_{C2}^2 + Q_{C2}^2)R_{eq2}}{V_{C2}^2} \tag{6}$$

$$Q_{S2} = Q_{C2} + \frac{(P_{C2}^2 + Q_{C2}^2)X_{eq2}}{V_{C2}^2} \tag{7}$$

where

$$P_{C2} = -(P_{C1} - \frac{P_{C1}^2 R_d}{U_{d1}^2})$$

By substituting equations (1)-(4) into the NR power flow iteration, the fundamental power flow of the hybrid system can be calculated.

B. Harmonic Model of the VSCs

From the earlier equations, one can see that when P_{ref} and Q_{ref} are determined, the power on both sides of the HVDC can be calculated under a certain firing angle. State-of-the-art research have studied the steady-state harmonic model of the VSC-HVDC transmission systems. The relationship between the three-phase injection voltage and injection current from both sides of the PCC is established as below [28], [31]

$$\begin{bmatrix} V_{S1} \\ V_{S2} \end{bmatrix} = \begin{bmatrix} A & B \\ C & D \end{bmatrix} \begin{bmatrix} I_{S1} \\ I_{S2} \end{bmatrix}$$

In most of the existing literature, the derivation of the ABCD mathematical formulae are based on the static synchronous compensator (STATCOM). Such ABCD models in [28] could not be applied for the proposed 2-level NSPWM controlled bi-terminal VSC-HVDC system. Considering the fact that the ABCD method could be extremely complex for re-derivation of the coefficients including the Bessel function and the Toeplitz matrix, another harmonic model for VSCs called the real harmonic coupling matrix (RHCM), which is based on the trigonometric-form Fourier series and piecewise-constant switching functions [10], is applied here.

The general harmonic coupling equation (HCE) $Y = KX$ represents the non-linear relationship of the AC/DC voltage and current in frequency domain. The coefficient matrix K is defined as the RHCM. K is the real-valued coefficient matrix, the specific expression of which is not listed here due to space limitations, but can be found in [10].

The kth harmonic voltage (k=1,2,3,$\cdots$,h) and the injected current of the AC and DC buses are

$$\begin{cases} I_{AC,i}^{(k)} = a_i^{(k)} + jb_i^{(k)} \\ a_i^{(k)} = \sum_{j\in i}(G_{AC,ij}^{(k)} e_j^{(k)} - B_{AC,ij}^{(k)} f_j^{(k)}) \\ b_i^{(k)} = \sum_{j\in i}(B_{AC,ij}^{(k)} e_j^{(k)} + G_{AC,ij}^{(k)} f_j^{(k)}) \end{cases} \tag{8}$$

$$\begin{cases} I_{DC,i}^{(k)} = c_i^{(k)} + jd_i^{(k)} \\ c_i^{(k)} = \sum_{j\in i}(G_{DC,ij}^{(k)} u_j^{(k)} - B_{DC,ij}^{(k)} v_j^{(k)}) \\ d_i^{(k)} = \sum_{j\in i}(B_{DC,ij}^{(k)} u_j^{(k)} + G_{DC,ij}^{(k)} v_j^{(k)}) \end{cases} \tag{9}$$

wherein G and B are elements in the kth harmonic nodal admittance matrices of the AC and DC networks

$$\begin{cases} Y_{AC}^{(k)} = G_{AC}^{(k)} + jB_{AC}^{(k)} \\ Y_{DC}^{(k)} = G_{DC}^{(k)} + jB_{DC}^{(k)} \end{cases}$$

And the relationship between AC and DC harmonic currents in the RHCM approach is

$$I_{DC}^{(k)} = K_I^{(k)} I_{AC}^{(k)} = (K_{ac}^{(k)} + K_{bc}^{(k)} P^{(k)}) I_{AC}^{(k)}$$
$$P^{(k)} = diag\{e^{jh\alpha} \cdots e^{j2\alpha}, e^{j\alpha}, 1, e^{-j\alpha}, e^{-j2\alpha} \cdots e^{-jh\alpha}\}$$

Similarly, the relationship between the AC and DC harmonic voltage in the RHCM is

$$V_{AC}^{(k)} = e^{(k)} + jf^{(k)} = K_V^{(k)} V_{DC}^{(k)} = K_{ab}^{(k)} V_{DC}^{(k)}$$
$$V_{DC}^{(k)} = u^{(k)} + jv^{(k)} = (K_{ab}^{(k)})^{-1} V_{DC}^{(k)}$$

Hence, by applying the RHCM method, harmonic voltage and current between the AC and DC sides of the VSC could be presented in a linear relationship. With the assumptions mentioned in Section II-A, VSCs are considered as the only harmonic source in the system. Hence, the imaginary parts of the DC quantities (k=0) are zeros, and the harmonic current injections $I_{AC}^{(k)}$ (k=2,3,$\cdots$,h) of the non-converter AC buses are zeros. The non-linear load expression of the VSC to calculate the harmonics is listed in Section III-A. With the relationship between the AC and DC harmonic currents and harmonic voltages at both ends of the VSC being characterized, the harmonic admittance matrix under specific harmonics could be established correspondingly.

Throughout the process, the harmonics are mainly affected by the coefficient matrix K, which is directly related to the applied switching function. Therefore, constructing an appropriate switching function using the method in Section II-B is important to ensure the accuracy of the results.

C. The VSC-HVDC HPF via A Unified NR Method

As shown in Figure 5, the flowchart of the proposed adaptive HPF algorithm consists of two loops. The calculation process of the HPF is similar to that of the continuation power flow (CPF), where the results of the CPF are regarded as the HPF under the 1st harmonic order. The admittance matrix under each harmonic order can be built through the RHCM method, and the HPF under each harmonic order could be obtained eventually. The initial values of the variables would directly affect the convergence of the NR method. However, the real and imaginary parts of the harmonics are very difficult to estimate. In this study, the VSC modulation variables $(m_a, \Delta\delta_1)$ in LOOP 2 were initialized from CPF in LOOP 1. In this way, the iteration of the HPF could achieve convergence no matter how the firing angle of the VSC changes, thereby realizing an *adaptive HPF*.

D. Conventional Equivalent Model for Validation

In order to verify the accuracy of the proposed framework, an equivalent model is built for performance comparison; that is, the hybrid AC/DC system is converted to an AC system. Specifically, with the power flow of the hybrid system under a firing angle being assessed, the power injected from both sides of the VSC-HVDC, i.e. $P_{S1} + jQ_{S1}$ and $P_{S2} + jQ_{S2}$, are substituted into the new load power on each side, and then the power flow runs without the VSC-HVDC station.

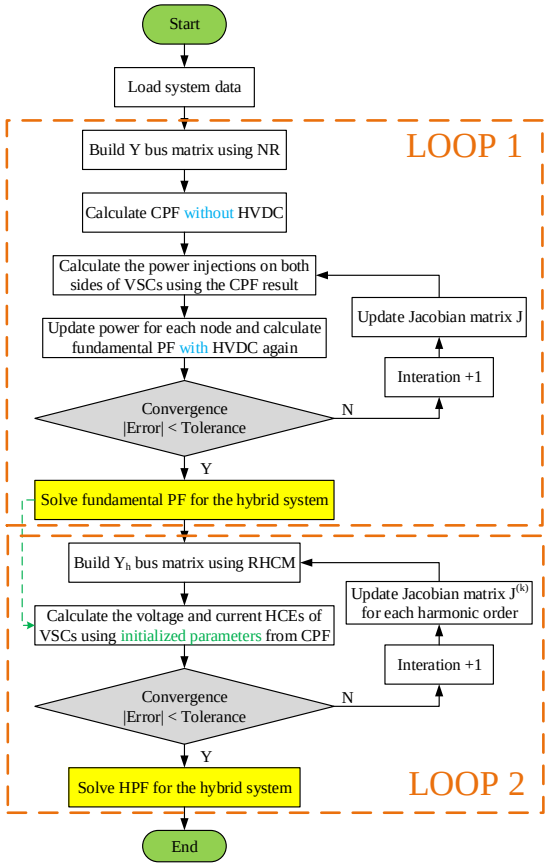

Fig. 5. Flowchart of the HPF algorithm applied to the 30-HVDC system.

IV. Numerical Case Study

A. A Hybrid AC/DC System Testbed

Figure 6 shows the single-line diagram of the developed 30-HVDC system. The parameters of the IEEE 30-bus transmission system are extracted from the Illinois Center for a Smarter Electric Grid (ICSEG) power world model [34].

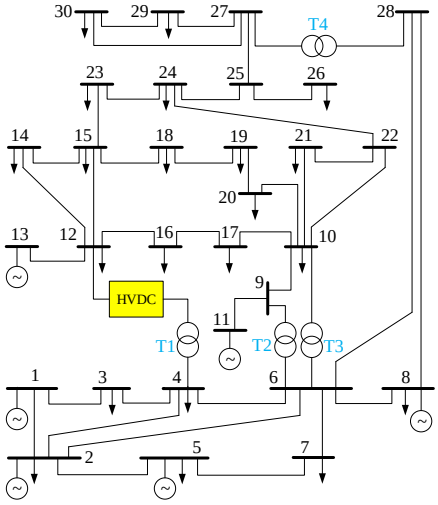

Fig. 6. Single-line diagram of the developed 30-HVDC system.

Analyzing the load flow of the original IEEE 30-bus system, the HVDC station, which is regarded as the harmonic source,

TABLE II
POWER FLOW OF THE SENDING-END AND RECEIVING-END UNDER DIFFERENT INJECTION POWERS

S_{ref} (MVA)	Firing Angle	S-Load Node 4	Sending-end transmitted	S-Load Node 12	Receiving-end consumed
$0+j0$	0°	$7.6+j1.6$	-	$11.2+j7.5$	-
$5+j1$	-0.7687°	$2.5989+j0.5294$	$5.0011+j1.0706$	$11.2013+j8.6583$	$0.0013+j1.1583$
$5+j10$	-0.7293°	$2.5944-j8.7573$	$5.0056+j10.3573$	$11.2072+j18.3636$	$0.0072+j10.8636$
$10+j1$	-1.5392°	$-2.4043+j0.3254$	$10.0043+j1.2746$	$11.2051+j9.1124$	$0.0051+j1.6124$
$10+j10$	-1.4816°	$-2.4090-j8.9722$	$10.0090+j10.5722$	$11.2114+j18.8790$	$0.0114+j11.3790$
$15+j1$	-2.3089°	$-7.4097-j0.0153$	$15.0097+j1.6153$	$11.2113+j9.8673$	$0.0113+j2.3673$
$15+j10$	-2.2331°	$-7.4146-j9.3312$	$15.0146+j10.9312$	$11.2185+j19.7379$	$0.0185+j12.2379$
$20+j1$	-3.0774°	$-12.4172-j0.4936$	$20.0172+j2.0936$	$11.2201+j10.9253$	$0.0201+j3.4253$
$20+j10$	-2.9836°	$-12.4225-j9.8354$	$20.0225+j11.4354$	$11.2285+j20.9457$	$0.0285+j13.4457$

should be set between node 4 and node 12. This is because the difference between the power flow and optimal power flow in these two nodes is the greatest among all the nodes.

B. Fundamental Power Flow

In this paper, the proposed method is to calculate the power of transformer-side first, and then update the power of each node into the NR method iteration. When the power on both sides of the VSC is determined, the fundamental power flow result could be calculated. We focus on the bus 4 and bus 12 which are the two terminals of the HVDC station and are both PQ buses. It is known that the line voltage at bus 4 is higher than that of bus 12, so bus 4 is considered the sending-end and bus 12 is the receiving-end.

Table II shows the power flow variation at both terminals of the HVDC station under different injection powers (i.e., firing angles). The injection power constraints could be estimated by Equation (3). When there is no injection power, i.e. $S_{ref} = P_{ref} + Q_{ref} = 0 + j0$ MVA, the firing angle $\Delta\delta_1 = 0°$, the fundamental power flow results on this hybrid system are the same as those of the IEEE 30-bus transmission system without VSC-HVDC station. When active injection power P_{ref} increases, the sending-end transmitted more corresponding active power, but the active power consumed by the receiving-end remains basically unchanged. When reactive injection power Q_{ref} increases, both the sending-end and receiving-end transmitted/consumed the corresponding reactive power.

As for verifying the CPF algorithm proposed in Section III-A, Figure 7 shows the comparison of three different types of fundamental power flow algorithms. The x-axis represents each node in the power grid, and the y-axis represents the voltage magnitude in per unit. The blue line segments stand for the actual data generated from MATLAB/Simulink hybrid system model (Figure 6). The gray line segments stand for the estimated data generated from the proposed algorithm. The orange line segments stand for the validation data generated from the conventional equivalent power grid in Section III-D. It is obvious that the proposed adaptive approach provides estimates much closer to the actual data.

C. Harmonic Power Flow

Figure 8 shows the voltage harmonics of the 30-HVDC system under a specific firing angle adjusted by the injection power of $S_{ref} = 5 + j1$ MVA. As shown in the chart,

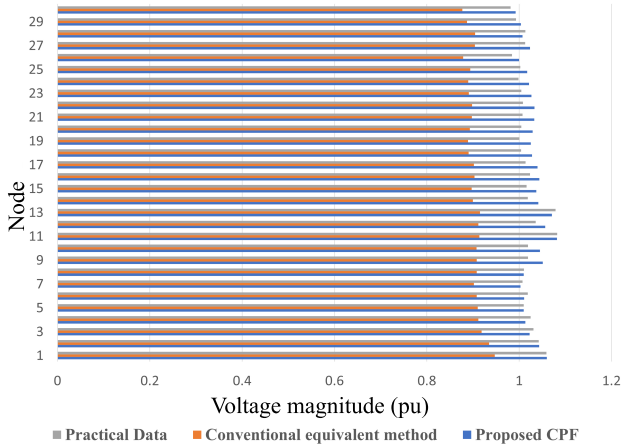

Fig. 7. Fundamental power flow comparison when $S_{ref} = 5 + j1$ MVA

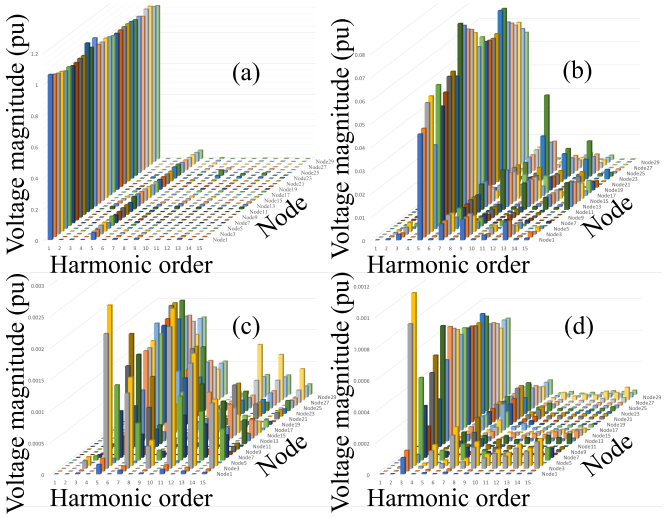

Fig. 8. Voltage harmonic magnitude comparison when $S_{ref} = 5 + j1$ MVA

the x-axis represents harmonic orders, the y-axis represents each node in the power grid, and the z-axis represents the per-unit voltage magnitude in frequency domain. Figure 8(a) shows the harmonics of the 30-HVDC system during the system operation. It is obvious that the magnitude at odd harmonics is larger, especially at the 5th harmonic. This is because the voltage magnitude at fundamental frequency is too large. Figure 8(b), (d), and (d) demonstrate the magnitude of subsequent harmonics for better comparison.

Figure 8(b) is the chart of Figure 8(a) with the magnitude at fundamental frequency removed. Figure 8(c) shows the voltage harmonics of the validation test method in Section III-D, which only considers the injected power on both sides of the VSC as an equivalent model. It ignores the interaction of two VSCs in the bi-terminal VSC-HVDC transmission station; so compared to Figure 8(b), the harmonics do not match.

Figure 8(c) shows the voltage harmonics of the 30-HVDC system using the proposed HPF algorithm. Compared to Figure 8(b), although some details are not aligned, the general estimation trend is in line with the actual harmonics (see, for example, the 5th and the 9th harmonic magnitude). The reason for the deviation may be that the method proposed in this paper and the calculations performed only consider VSC as a harmonic source (see the assumptions in Section II-D). There are many more harmonic sources in the actual power system such as transformers, regulators, and the PI control strategies that would also affect the harmonics injection and propagation throughout the network [35].

V. Conclusion

In this paper, an adaptive HPF algorithm based on a bi-terminal VSC-HVDC transmission system is proposed. The power flow analysis of the AC/DC hybrid system is realized by iterating the switching function and building the harmonic voltage and current RHCM relationship of the VSC at both ends. Experiments demonstrated that the proposed method features high accuracy in solving the power flow in hybrid AC/DC systems with VSC-HVDC where harmonics are dominant. Future research may be targetted to improve the harmonic analysis accuracy under more intensive presence of harmonic sources in modern power systems, either imposed internally via the power system equipment or externally through solar storms and the resulting geomagnetic disturbances.

References

[1] E. Acha and M. Madrigal, *Power System Harmonics: computer modelling and analysis*. John Wiley, 2001.

[2] D. Jovcic and K. Ahmed, "VSC-HVDC applications and topologies, performance and cost comparison with LCC HVDC," *High Voltage Direct Current Transmission Converters, Systems and DC Grids*, pp. 123–140, 2015.

[3] P. Nguyen and M. Han, "Study on harmonic propagation of VSC-based HVDC systems," in *2014 International Conference on Power System Technology*. IEEE, 2014, pp. 2146–2153.

[4] K. Olejniczak and G. T. Heydt, "Basic mechanisms of generation and flow of harmonic signals in balanced and unbalanced three-phase power systems," *IEEE Power Eng. Review*, vol. 9, no. 10, pp. 58–58, 1989.

[5] M. P. Bahrman, "Overview of HVDC transmission," in *2006 IEEE PES Power Systems Conference and Exposition*. IEEE, 2006, pp. 18–23.

[6] L. Gengyin, Z. Ming, H. Jie, L. Guangkai, and L. Haifeng, "Power flow calculation of power systems incorporating VSC-HVDC," in *2004 International Conference on Power System Technology, 2004. PowerCon 2004.*, vol. 2. IEEE, 2004, pp. 1562–1566.

[7] M. Baradar and M. Ghandhari, "A multi-option unified power flow approach for hybrid AC/DC grids incorporating multi-terminal VSC-HVDC," *IEEE Trans. Power Syst.*, vol. 28, no. 3, pp. 2376–2383, 2013.

[8] R. Chai, B. Zhang, J. Dou, Z. Hao, and T. Zheng, "Unified power flow algorithm based on the nr method for hybrid AC/DC grids incorporating VSCs," *IEEE Trans. on Power Syst.*, vol. 31, no. 6, pp. 4310–4318, 2016.

[9] Q. Zhong, L. Lin, G. Wang, Y. Zhang, and Z. Wu, "Harmonic analysis model for voltage source converter under unbalanced conditions," *IET Generation, Transmission & Distribution*, vol. 9, no. 1, pp. 12–21, 2015.

[10] B. Liu, Z. Du, and C. Li, "Harmonic power flow of VSC-HVDC based AC/DC power systems," *Electric Power Systems Research*, vol. 133, pp. 355–364, 2016.

[11] H. M. Ahmed, A. B. Eltantawy, and M. Salama, "A generalized approach to the load flow analysis of AC-DC hybrid distribution systems," *IEEE Transactions on Power Systems*, vol. 33, no. 2, pp. 2117–2127, 2017.

[12] R. Chen, J. Niu, H. Gui, Z. Zhang, F. Wang, L. M. Tolbert, B. J. Blalock, D. J. Costinett, and B. B. Choi, "Analytical analysis of AC and DC side harmonics of three-level active neutral point clamped inverter with space vector modulation," in *2019 IEEE Applied Power Electronics Conference and Exposition (APEC)*. IEEE, 2019, pp. 112–119.

[13] W. Ahmed and S. M. U. Ali, "Comparative study of SVPWM (space vector pulse width modulation) & SPWM (sinusoidal pulse width modulation) based three phase voltage source inverters for variable speed drive," in *IOP Conference Series: Materials Science and Engineering*, vol. 51, no. 1. IOP Publishing, 2013, p. 012027.

[14] S. Bowes and B. Bird, "Novel approach to the analysis and synthesis of modulation processes in power convertors," in *Proceedings of the Institution of Electrical Engineers*, vol. 122, no. 5. IET, 1975, pp. 507–513.

[15] D. G. Holmes and T. A. Lipo, *Pulse width modulation for power converters: principles and practice*. John Wiley & Sons, 2003, vol. 18.

[16] "Back to back converter," Typhoon HIL Documentation, [Online] Available at: https://www.typhoon-hil.com/documentation/typhoon-hil-software-manual/References/back_to_back_converter.html, Accessed:2021.

[17] W. Bai, M. R. Abedi, and K. Y. Lee, "Distributed generation system control strategies with PV and fuel cell in microgrid operation," *Control Engineering Practice*, vol. 53, pp. 184–193, 2016.

[18] T. L. Van and D.-C. Lee, "Developing function models of back-to-back PWM converters for simplified simulation," *Journal of Power Electronics*, vol. 11, no. 1, pp. 51–58, 2011.

[19] "LCL filters instructions manual," CIRCUTOR, [Online] Available at: http://docs.circutor.com/docs/M98121701-03.pdf, Accessed:2021.

[20] S. Ademi, D. Tzelepis, A. Dysko, S. Subramanian, and H. Ha, "Fault current characterisation in VSC-based HVDC systems," 2016.

[21] E. Krige, "Harmonic interaction between weak AC systems and VSC-based HVDC schemes," Ph.D. dissertation, Stellenbosch: Stellenbosch University, 2012.

[22] N. Mohan, T. M. Undeland, and W. P. Robbins, *Power electronics: converters, applications, and design*. John wiley & sons, 2003.

[23] C. Zheng, X.-x. Zhou, R.-m. Li, and C.-h. SHENG, "Study on the steady characteristic and algorithm of power flow for VSC-HVDC," *Proceedings of the CSEE*, vol. 25, no. 6, pp. 1–5, 2005.

[24] G. Wang, Y. Cai, G.-b. ZHANG, and Z. Xu, "Equivalent model of HVDC-VSC and its hybrid simulation technique," *Power system technology*, vol. 2, 2003.

[25] Z. Guibin, X. Zheng, and W. Guangzhu, "Steady-state model and its nonlinear control of VSC-HVDC system," *Proceedings-Chinese Society of Electrical Engineering*, vol. 22, no. 1, pp. 17–22, 2002.

[26] "PWM generator (2-level)," MathWorks, [Online] Available at: https://www.mathworks.com/help/physmod/sps/powersys/ref/pwmgenerator2level.html, Accessed:2021.

[27] B. LIU and Z. DU, "Unified Newton's solution to three-phase harmonic power flow of VSC-HVDC based AC/DC power systems," *Proceedings of the CSEE*, 2018.

[28] M. M. Martinez, "Modelling of power electronics controllers for harmonic analysis in power systems," Ph.D. dissertation, University of Glasgow, 2001.

[29] E. Karami, M. Madrigal, and G. Gharehpetian, "Dynamic harmonic modeling and analysis of VSC-HVDC systems," *AUT Journal of Electrical Engineering*, vol. 49, no. 1, pp. 31–38, 2017.

[30] C. Zheng, X.-x. Zhou, R.-m. Li *et al.*, "Dynamic modeling and transient simulation for voltage source converter based HVDC," *Power System Technology*, vol. 29, no. 16, pp. 1–5, 2005.

[31] M. Madrigal and E. Acha, "Harmonic modelling of voltage source converters for HVDC stations," 2001.

[32] B. Wu and M. Narimani, *High-power converters and* AC *drives*. John Wiley & Sons, 2017.

[33] "IEEE recommended practice and requirements for harmonic control in electric power systems," *IEEE Std 519-2014 (Revision of IEEE Std 519-1992)*, pp. 1–29, 2014.

[34] "IEEE 30-bus system," Illinois Center for a Smarter Electric Grid, [Online] Available at: https://icseg.iti.illinois.edu/ieee-30-bus-system/, Accessed:2021.

[35] C. Zhao, Y. Hu, K. Luan, F. Xu, Z. Li, P. Wang, and Y. Li, "Energy storage requirements optimization of full-bridge mmc with third-order harmonic voltage injection," *IEEE Transactions on Power Electronics*, vol. 34, no. 12, pp. 11 661–11 678, 2019.